




## Three-dimensional isotropic droplets in Rydberg-dressed Bose gases

Hao Zhu <sup>1</sup>, Yu-Quan Ma,<sup>2</sup> Wen-Kai Bai,<sup>1</sup> Yan-Mei Yu,<sup>1</sup> Fang-Fu Ye,<sup>3,4,5</sup> Yong-Yao Li <sup>6,\*</sup>  
Lin Zhuang,<sup>7,†</sup> and Wu-Ming Liu <sup>1,4,5,‡</sup>

<sup>1</sup>Beijing National Laboratory for Condensed Matter Physics, Institute of Physics, Chinese Academy of Sciences, Beijing 100190, China

<sup>2</sup>School of Applied Science, Beijing Information Science and Technology University, Beijing 100192, China

<sup>3</sup>Beijing National Laboratory for Condensed Matter Physics and Laboratory of Soft Matter Physics, Institute of Physics, Chinese Academy of Sciences, Beijing 100190, China

<sup>4</sup>School of Physical Sciences, University of Chinese Academy of Sciences, Beijing 100190, China

<sup>5</sup>Songshan Lake Materials Laboratory, Dongguan, Guangdong 523808, China

<sup>6</sup>Guangdong-Hong Kong-Macao Joint Laboratory for Intelligent Micro-Nano Optoelectronic Technology, School of Physics and Optoelectronic Engineering, Foshan University, Foshan 528225, China

<sup>7</sup>School of Physics, Sun Yat-Sen University, Guangzhou 510257, China



(Received 2 May 2023; accepted 18 April 2024; published 10 May 2024)

We predict a scheme for the creation of isotropic three-dimensional quantum droplets in Rydberg-dressed Bose gases, which contain both repulsive contact interactions and attractive soft-core interactions. Via manipulating laser detuning, the droplet size and particle number density could be engineered. Quantum fluctuation induced Lee-Huang-Yang (LHY) correction should be considered to stabilize droplets when LHY energy is comparable to the mean-field energy. Self-trapped droplets possess flat-top density distribution for a large particle number, and the collective excitations are calculated to determine the self-evaporation threshold. We further distinguish quantum droplets from solitons according to condensate compressibility. Finally, the dynamic stability of droplets is examined by pairwise-droplet collision. Our system could realize the most dilute quantum droplets, and establish a promising platform for further simulating topological nontrivial droplets.

DOI: [10.1103/PhysRevResearch.6.023151](https://doi.org/10.1103/PhysRevResearch.6.023151)

### I. INTRODUCTION

Quantum droplets represent the most dilute liquid, in which the atom number density is  $10^8$  times lower than in a liquid helium [1,2]. Recently, three-dimensional (3D) droplets have attracted much attention in ultracold Bose gases where the mean-field-driven collapse is prohibited by a repulsive interaction arising from quantum fluctuation [2–4]. Since mean-field (MF) theory cannot explain the stability of droplets against collapse [5], beyond mean-field (BMF) theory with the quantum fluctuation induced Lee-Huang-Yang (LHY) correction is employed to explain microscopic droplets [6–8]. Currently, droplets in Bose-Einstein condensates (BECs) can be roughly divided into two categories: (1) single component magnetic gases, in which the MF effect is given by dipolar and contact interactions, rendering droplets to exhibit an elongated filament shape [9–15], and (2) binary mixtures of two spin components or heteronuclear atoms, with almost complete cancellation of the MF effect, leaving a small residual attraction compensated by repulsive LHY energy [16–20].

Through manipulating short-range contact interactions by Feshbach resonance, droplet sizes can reach nearly  $10\ \mu\text{m}$  [21–24]. Recent work relating to soliton-droplet transitions [25,26], rotating droplets [27,28], and collective excitations in droplets [29–32] yields that quantum droplets are outstanding microscopic platforms for studying topology and superfluid, whereas searching for macroscopic droplets suggests more remarkable application potentials.

Resonantly excited Rydberg gases enable researchers to systematically study strong interactions in large-size systems, while its short lifetime hinders experimental engineering [33–35]. This shortcoming can be circumvented by weakly dressing the atomic ground state with a small fraction of Rydberg state that improves the overall lifetime of the system [36]. Especially, the coupling between the ground state and  $nS$  Rydberg exciting state is conceived to introduce repulsive soft-core interactions with effective coupling parameter  $\tilde{C}_6 > 0$  and red detunings, which can lead to supersolid states [37–40]. Moreover, with  $\tilde{C}_6 < 0$  and blue detunings, attractive soft-core interactions dominate the system [41–44], where solitons are generated [45]. However, whether quantum fluctuation could play an important role in this system remains an important question.

In this paper, we utilize beyond mean-field theory to predict three-dimensional isotropic droplets in  $^{87}\text{Rb}$  Rydberg-dressed gases, in which the droplet size can reach  $100\ \mu\text{m}$ . Via manipulating interaction ratio and particle number, it is possible to realize stable droplets where MF energy is negative while LHY energy is positive. We develop the beyond Gross-Pitaevskii equation (BGPE) for single-component

\*yongyaoli@gmail.com

†stszhl@mail.sysu.edu.cn

‡wliu@iphy.ac.cn

Published by the American Physical Society under the terms of the [Creative Commons Attribution 4.0 International](https://creativecommons.org/licenses/by/4.0/) license. Further distribution of this work must maintain attribution to the author(s) and the published article's title, journal citation, and DOI.

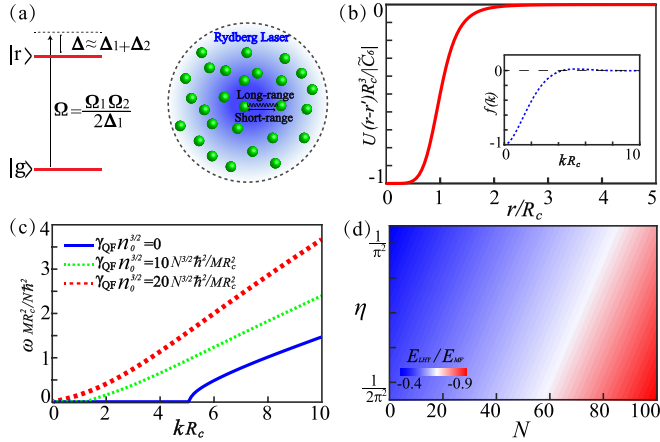


FIG. 1. (a) Rydberg-dressed states can be realized by imposing BECs into Rydberg laser. Atoms in BECs interact through MF interactions, including both repulsive short-range and attractive long-range interactions. Level scheme of the considered Rydberg-dressed approach contains ground-state  $|g\rangle$ , Rydberg state  $|r\rangle$ , with Rydberg laser frequency  $\Omega$  and blue detuning  $\Delta$ . (b) Attractive long-range interaction between Rydberg-dressed atoms  $U(\mathbf{r}-\mathbf{r}')$  is referred to as soft-core interaction. The inset displays the Fourier transformation of the soft-core interaction  $f(k)$ , where the minimum of the interaction is located at  $k=0$  with  $R_c$  representing Rydberg radius. (c) Schematic showing the effect of LHY correction  $\gamma_{QF} n_0^{3/2}$  on the excitation spectra  $\omega$ , where  $n_0$  represents particle number density. (d) LHY energy relative to MF energy, where  $\eta$  equals to the ratio of soft-core interaction as well as contact interaction and  $N$  is the particle number.

Rydberg-dressed gases, and self-evaporation region of droplets is determined through collective mode calculation. When compared to solitons, droplets exhibit totally different compressibility, and the droplet size can be freely tuned by laser detunings. Finally, the phase diagram of droplets is summarized and the collide dynamic of flat-top droplets indicates a long lifetime to be engineered in experiments.

## II. RYDBERG-DRESSED SYSTEM AND BEYOND GROSS-PITAEVSKII EQUATION

The Rydberg-dressed approach is based on optical dressing of ground-state  $|g\rangle$  atoms onto highly excited Rydberg states  $|r\rangle$  with Rydberg lasers, as illustrated by the simplified two-level model in Fig. 1(a). The blue detuning  $\Delta \approx \Delta_1 + \Delta_2$  and Rabi frequency  $\Omega = \frac{\Omega_1 + \Omega_2}{2\Delta_1}$ , with  $\Omega_{1,2}$  and  $\Delta_{1,2}$  representing Rabi frequencies and detuning in the two-photon dressing scheme. Hence, it will mix a small fraction  $\nu = (\Omega/2\Delta)^2$  of Rydberg-state atoms into ground-state atoms [37,46,47]. Balanced by repulsive short-range interactions, attractive long-range interactions are believed to stabilize the condensate from dissipation. Inspired by the recent research on droplets induced by the balance between MF and LHY energy [2,8,48], we will prove the existence of quantum droplets in Rydberg-dressed system.

We consider  $N$  Rydberg-dressed atoms interacting through both repulsive contact and attractive soft-core interactions. The time-independent ground-state wave function  $\Psi_0$  satisfies the equation  $\mu\Psi_0 = \mathcal{L}_{GP}\Psi_0$ , where  $\mu$  is the chemical

potential and  $\mathcal{L}_{GP} = -\frac{\hbar^2\nabla^2}{2M} + \Phi(\mathbf{r})$ . The effective potential  $\Phi(\mathbf{r}) = g\delta(\mathbf{r}-\mathbf{r}') + \int d^3\mathbf{r}' U(\mathbf{r}-\mathbf{r}')|\Psi_0(\mathbf{r}')|^2$  describes two-body interactions, in which the coupling constant  $g = \frac{4\pi\hbar^2 a_s}{M}$  is related to  $s$ -wave scattering length  $a_s$ . The attractive long-range potential  $U(\mathbf{r}-\mathbf{r}') = \frac{\tilde{C}_6}{R_c^6 + |\mathbf{r}-\mathbf{r}'|^6}$  is depicted in Fig. 1(b), with soft-core constant  $\tilde{C}_6 < 0$  and  $R_c$  representing the blockade radius [41–43]. Fourier transformation of the soft-core potential reads  $U(k) = U_0 f(k)$ , where  $U_0 = \frac{2\pi^2|\tilde{C}_6|}{3R_c^3}$  identifies the strength and  $f(k)$  has an analytical form  $f(k) = -e^{-kR_c/2}[e^{-kR_c/2} - 2\sin(\pi/6 - \sqrt{3}kR_c/2)]/kR_c$ , which characterizes the momentum dependence of the interaction [inset of Fig. 1(b)]. Thereby, the minimum value of the effective potential  $\Phi(k) = g + U(k)$  locates at  $k=0$ .

Considering the particle number of  $60S$  state  $^{87}\text{Rb}$  atoms  $N \leq 10^4$ , the number of Rydberg-state atoms is controlled by Rabi frequency  $\Omega$  and laser detuning  $\Delta$  via  $N_r = N\nu \leq 1$ . The Rydberg blockade radius approximates  $3\mu\text{m}$  in our system, which is comparable to the healing length. Consequently, quantum fluctuation in our system stems from the atoms where both short-range interactions and soft-core interaction are considered. The LHY correction parameter can then be obtained from the zero-point quantum fluctuation of all quasiparticle modes [49]. Based on the Bogoliubov-de Gennes (BdG) equation, the excitation spectrum of a 3D uniform Rydberg-dressed condensate can be given by  $\omega = \sqrt{\frac{\hbar^2 k^2}{2M}(\frac{\hbar^2 k^2}{2M} + 2n_0\Phi(k) + 3\gamma_{QF}n_0^{3/2})}$  [50]. As shown in Fig. 1(c), the imaginary part of the excitation spectrum can be canceled by higher particle number density with LHY correction, indicating stability when considering quantum fluctuation.

The time-dependent BGPE can be transformed into dimensionless form as

$$i\frac{\partial\Psi(\mathbf{r},t)}{\partial t} = \left[-\frac{1}{2}\nabla^2 + \Phi(\mathbf{r},t) + \gamma_{QF}|\Psi(\mathbf{r},t)|^3\right]\Psi(\mathbf{r},t), \quad (1)$$

where  $\Phi(\mathbf{r},t) = \alpha|\Psi(\mathbf{r},t)|^2 - \gamma\int d\mathbf{r}'\frac{|\Psi(\mathbf{r}',t)|^2}{1-|\mathbf{r}-\mathbf{r}'|^6}$  with contact interaction  $\alpha = \frac{gMN}{\hbar^2 R_c}$ , soft-core interaction  $\gamma = \frac{|C_6|MN}{\hbar^2 R_c^4}$ , and LHY correction  $\gamma_{QF} = \frac{4M^{3/2}(g-2\pi^2|C_6/3R_c^3|)^{5/2}}{3\pi^2\hbar^3}$ . To study properties of droplets, we solve Eq. (1) in imaginary time [51–53]. The parameter  $\eta = \gamma/\alpha$  compares the strength of long-range attractive interaction and repulsive contact interaction. The corresponding energy functional can be expressed as  $E = E_{MF} + E_{LHY}$ , where MF energy  $E_{MF} = \int[\frac{1}{2}|\nabla\Psi(\mathbf{r})|^2 + \frac{1}{2}\alpha|\Psi(\mathbf{r})|^2]d\mathbf{r} - \frac{1}{2}\gamma\int[\frac{1}{1+|\mathbf{r}-\mathbf{r}'|^6}|\Psi(\mathbf{r})|^2|\Psi(\mathbf{r}')|^2]d\mathbf{r}d\mathbf{r}'$  and LHY energy  $E_{LHY} = \frac{2}{5}\int[\gamma_{QF}|\Psi(\mathbf{r})|^5]d\mathbf{r}$ . Fig. 1(d) suggests that LHY energy shares an opposite symbol from MF energy, where interaction ratio  $\eta$  and particle number  $N$  are changed, guaranteeing  $E_{LHY}/E_{MF}$  negative. Meanwhile, LHY energy and MF energy are in the same order, suggesting LHY correction should not be neglected [3].

## III. MACROSCOPIC DROPLETS WITH TUNABLE SIZES

For a fixed interaction ratio, the droplet solutions are obtained for different particle numbers  $N$  from Eq. (1) via the imaginary-time propagation method. One-dimensional density distribution of the droplet is exhibited in the

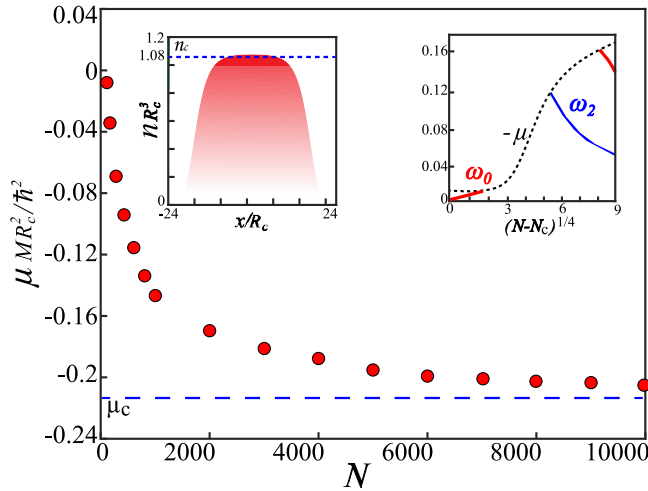


FIG. 2. Chemical potential  $\mu$  of droplets as a function of particle number  $N$ , where  $\mu$  approximates the critical value  $\mu_c = -0.215$  (blue dashed line) for large  $N$ . Left inset: One-dimensional density profile of the droplet with  $N = 10^4$  along the  $x$  direction, where the peak value approximates the critical value  $n_c = 1.08$  (blue dotted line). Right inset: Particle emission and excitation spectrum with different angular momentum  $\omega_l$  ( $l = 0, 2, \dots$ ) are displayed in the right panel, where  $N_c = 95$ .

left-panel inset of Fig. 2, where the particle number  $N = 10^4$ . The particle number density maintains constant in the central area while drops rapidly at the condensate edge, which represents the flat-top droplet. One can therefore apply the Thomas-Fermi (TF) approximation to analyze them, i.e., neglecting the contribution from the kinetic term [54]. Consequently, energy of the system can be written as  $E = \frac{1}{2}[-\epsilon n_0^2 + \alpha n_0^2 + \frac{4}{3}\gamma_{\text{QF}}n_0^{5/2}]V$ , where  $V = N/n_0$  denotes the volume of the droplet,  $n_0 = |\Psi(\mathbf{r}, t)|^2$  is the ground-state particle number density,  $N$  is the total particle number, and  $\epsilon = \gamma \int \frac{1}{1+|r-r'|^6} d\mathbf{r}d\mathbf{r}'$  is the long-range attraction effect. When the system is in equilibrium with quantum pressure  $\frac{dE}{dn_0} = 0$ , we have  $\sqrt{n_0} = -\frac{5}{6\gamma_{\text{QF}}}(\alpha - \epsilon)$ . Substituting  $\epsilon \approx 6.6\gamma$  into the aforementioned density, we obtain a critical peak density  $n_c = 1.08$ . Moreover, according to Eq. (1), we assume the solution  $\Psi(\mathbf{r}, t) = \Psi_0(\mathbf{r})e^{-i\mu t}$ . With the TF approximation, we can obtain the chemical potential at equilibrium  $\mu_c = (\alpha - \epsilon)n_0 + \gamma_{\text{QF}}n_0^{3/2} = -0.215$  (blue dashed line). Clearly, as shown in Fig. 2, the chemical potential  $\mu$  of droplets decreases with increasing particle number  $N$  towards the critical  $\mu_c$ . Furthermore, we note that the  $\mu(N)$  curve satisfies the necessary stability condition in the form of Vakhitov-Kolokolov criterion  $d\mu/dN < 0$  [55], and the chemical potential is always negative, implying the state is self-bound in equilibrium.

Besides self-bound behaviors, self-evaporation of droplets is also investigated in the right inset of Fig. 2. According to Bogoliubov theory, the excitations of the ground-state droplet solutions can be obtained by solving the BdG equations through linearizing Eq. (1) with respect to the fluctuation part  $\delta\Psi(\mathbf{r}, t)$  [2]. In the right inset of Fig. 2, we show the particle emission threshold  $-\mu$  (black dotted line) and the frequencies of different angular momentum modes  $\omega_l$  ( $l = 0, 2, \dots$ ), as functions of  $(N - N_c)^{1/4}$ . In the interval of

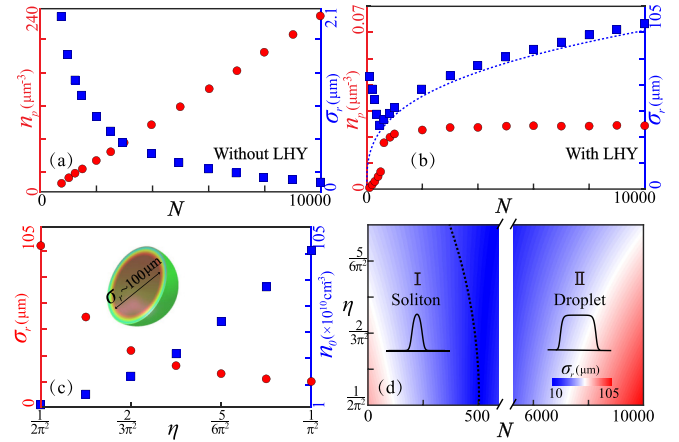


FIG. 3. (a) Peak density  $n_p$  and condensate width  $\sigma_r$  of solitons vary with particle number  $N$  without LHY correction, and the interaction ratio is fixed for different  $N$ . (b) Peak density  $n_p$  and droplet width  $\sigma_r$  vary with particle number  $N$  with LHY correction, and the interaction ratio is the same as the former soliton case. (c) The droplet size as large as  $100 \mu\text{m}$  can be manipulated by the interaction ratio for  $N = 10^4$ , and particle number density  $n_0$  is changed correspondingly. (d) Phase diagram of solitons (region I) and quantum droplets (region II), where the boundary is depicted by the black dashed line. The color-scale legend denotes the width of the condensate ranging from  $15 \mu\text{m}$  to  $105 \mu\text{m}$ .

$105 < N < 1080$ , there are no modes appearing below  $-\mu$ , suggesting the self-evaporation region of the droplet.

As the aforementioned discussion has reflected the importance of the LHY correction in stabilizing the droplet, we will further compare the compressibility of droplet solutions with the soliton results. When ignoring the LHY correction, solitons self-trapped by attractive soft-core interactions are believed to exist in the Rydberg-dressed system [45]. Density maximum of solitons can be identified by density peak  $n_p$ , as depicted in Fig. 3(a), where  $n_p$  raises linearly with increasing particle number  $N$ . On the contrary, the soliton width  $\sigma_r$  shrinks with  $N$ , which indicates the soliton is compressible (the width of the soliton can be extracted from the BGPE solutions employing  $\sigma_r^2 = c \int r |\Psi(\mathbf{r})|^2 d\mathbf{r}$ , where  $c$  is a normalization constant). When considering the LHY correction in Fig. 3(b), the density peak of the droplet raises with  $N$  towards the critical value  $n_c$ , then remains constant for larger  $N$ . On the other hand, the relationship between droplet sizes  $\sigma_r$  and particle numbers  $N$  is nonmonotonic. The condensate width decreases when  $N \leq 500$ , which implies compressible solitons. However,  $\sigma_r$  raises for larger  $N$ , and we could utilize the flat-top droplet model to explain this phenomenon theoretically. Through substituting the particle number density  $n_0$  into energy functional  $E$  and solving the equation  $dE/dV = 0$ , we can obtain the relationship between droplet volume and particle number  $V = \frac{36}{25}\gamma_{\text{QF}}^2 \frac{N}{(\alpha - \epsilon)^2}$ . Assuming the droplet is a 3D isotropic ball, we can easily find the relationship between  $\sigma_r$  and  $N$ :  $\sigma_r = \left[ \frac{27\gamma_{\text{QF}}^3 N}{25\pi(\alpha - \epsilon)^2} \right]^{1/3}$  (exhibited by blue dotted line, agreeing well with the numerical results). Considering



TABLE I. Comparison of size and particle number density.

|                                | $^{39}\text{K}$ [22] | $^{164}\text{Dy}$ [24] | Rydberg-dressed $^{87}\text{Rb}$ |
|--------------------------------|----------------------|------------------------|----------------------------------|
| $^a\sigma_r$ ( $\mu\text{m}$ ) | $\sim 3$             | $\sim 1$               | $\sim 100$                       |
| $^bn_0$ ( $\text{cm}^{-3}$ )   | $10^{15}$            | $10^{21}$              | $10^{10}$                        |

<sup>a</sup> $\sigma_r$  denotes the size of the droplet.

<sup>b</sup> $n_0$  denotes the particle number density of the droplet.

the nearly constant bulk density, flat-top droplets are incompressible.

We remark that the size of the 3D droplet in the Rydberg-dressed system exceeds  $100\ \mu\text{m}$  for a large particle number, i.e.,  $N = 10^4$ . The cut through the center of the profile reveals the characteristic flat-top density distribution, which agrees well with the density distribution known for liquid helium droplets. This kind of macroscopic droplet outdistances the size of droplets in binary or dipolar BECs, and the droplet size is manipulated only by the Rydberg laser detuning [21–24]. With different laser detuning frequency  $\Delta$ , the interaction ratio  $\eta = |\tilde{C}_6|/gR_c^3$  will change correspondingly. This phenomenon results in different-sized droplets ranging from  $15\ \mu\text{m} \sim 105\ \mu\text{m}$  for a fixed particle number  $N = 10^4$ , as exhibited in Fig. 3(c). Correspondingly, the particle number density  $n_0$  can also be tuned by  $\eta$ , which is far more dilute than binary or dipolar droplets (in Table I). Within this protocol, the competition between solitons and droplets is summarized in Fig. 3(d), where the condensate size is varied by interaction ratios  $\eta$  and particle numbers  $N$ . The phase diagram can be further divided into solitons (in region I) and quantum droplets (in region II), the boundary between which is depicted by black dashed line. From the perspective of one-dimensional density distribution, the soliton is Gaussian type while the quantum droplet possesses equal particle number density except at the boundary. In another vein, considering the condensate width  $\sigma_r$  decreases with  $N$  in region I while increasing in region II, we can conclude that the soliton is compressible whereas the quantum droplet is incompressible.

#### IV. DROPLET STABILITY FORM COLLISIONS

Experimentally, coherent Rydberg excitation of cold atoms has been demonstrated under various conditions [41–44]. To reveal the dynamic stability of droplets, we monitor the collision dynamic of pairwise droplets in Fig. 4. We adopt two flat-top droplets as initial states:  $\Psi(x, y, z, t = 0) = \Psi_1(x - x_0, y, z)e^{-ik_0x/2} + \Psi_2(x + x_0, y, z)e^{+ik_0x/2}$ , where  $\Psi_{1,2}$  are the ground-state solutions from BGPE with equal particle number  $N = 10^4$ ,  $\pm x_0$  are the initial positions of the two droplets, and  $k_0$  is the initial relative momentum of the colliding droplets. Similar to the collision of classical liquids, two outcomes of the collision of the quantum droplets are observed. For a relatively small collision velocity  $k_0 = 0.5$  in Fig. 4(a), the droplets merge into a single droplet upon colliding, which features an inelastic collision. However, for a larger collision velocity  $k_0 = 1$  in Fig. 4(b), the droplets separate again after merging, which suggests the collision approaches to be quasielastic. Collision of droplets in the Rydberg-dressed sys-

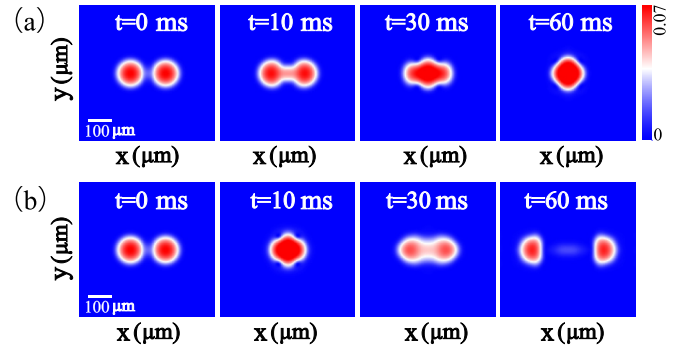


FIG. 4. Collision of two droplets in two-dimensional projection. (a) The initial collision velocity  $k_0 = 0.5\ \mu\text{m}^{-1}$ , inelastic collision emerges at  $t = 60$  ms. (b) The initial collision velocity  $k_0 = 1\ \mu\text{m}^{-1}$ , elastic collision emerges at  $t = 60$  ms

tem exhibits similar behavior as solitons [56], and the droplets could maintain the self-trapped property after collision.

#### V. CONCLUSION

We first propose the Rydberg-dressed system as a platform for realizing macroscopic droplets with over  $100\ \mu\text{m}$  size. The isotropy of droplets may be broken when considering  $nP$  or  $nD$  state Rydberg-dressing [57–59]. Quantum fluctuation effect, i.e., LHY correction, which transforms solitons into droplets, plays a vital role in stabilizing droplets when the LHY energy is comparable to the mean-field energy. The macroscale droplets can be generated by different Rydberg laser detuning rather than Feshbach resonance. Compressible solitons and incompressible droplets are summarized by the phase diagram. Finally, the collision of two flat-top droplets indicates long-lifetime stability of the droplets. Considering the potential applications of droplets to investigate superfluid or polaron physics [60,61], it is worth further introducing spin-orbit coupling [62,63] or spin-angular momentum [64] into the Rydberg-dressed droplets.

#### ACKNOWLEDGMENTS

We thank Dr. Y. H. Xing for valuable discussions. This paper was supported by the National Key R&D Program of China under Grants No. 2021YFA1400900, No. 2021YFA0718300, No. 2021YFA1402100, and No. 2021YFA1402104; NSFC under Grants No. 61835013, No. 12174461, No. 12234012, No. 12334012, No. 52327808, No. 11874064, No. 11934014, No. 12004392, and No. 12305029; Space Application System of China Manned Space Program, Strategic Priority Research Program of the Chinese Academy of Science (CAS) under Grant No. XDB21030300; and NKRD Program of China under Grant No. 2021YFA1402104.

#### APPENDIX A: EXPERIMENTAL PROPOSALS FOR REALIZING ATTRACTIVE SOFT-CORE INTERACTIONS

One of the major advantages of Rydberg atoms lies in its versatile controllability by choosing appropriate states [33–35]. Besides microwave, off-resonant laser dressing of Rydberg states provides an opportunity to realize soft-core

long-range interactions [36]. Off-resonant laser dressing could admix a small fraction of Rydberg state  $|r\rangle$  into the ground state  $|g\rangle$ , resulting in the dressed eigenstate  $|\Psi\rangle \sim |g\rangle + \nu|r\rangle$ . The Rydberg state proportion is manipulated by dressing parameter  $\nu \propto (\Omega/2\Delta)$ , where  $\Omega$  and  $\Delta$  stand for the Rabi frequency and detuning of the laser dressing field, respectively. Satisfying the requirements of a realistic experimental, Rydberg-dressed state can persist for an ultralong time. Assuming atoms in Rydberg states  $|r\rangle$  interact with each other through van der Waals (vdW) interaction  $C_6/|\mathbf{r}-\mathbf{r}'|^6$ , satisfying  $C_6\Delta > 0$ , two dressed ground-state atoms obtain a modified soft-core potential  $U(\mathbf{r}-\mathbf{r}') = \frac{\tilde{C}_6}{R_c^6+|\mathbf{r}-\mathbf{r}'|^6}$ , with  $\tilde{C}_6 = (\Omega/2\Delta)^4 C_6$  being the effective interaction coefficient and  $R_c = (C_6/2\hbar\Delta)^{1/6}$  standing for a blockade radius. When both  $C_6$  and  $\Delta$  are negative, the attractive soft-core potential  $U(\mathbf{r}-\mathbf{r}')$  can be understood as follows: when two atoms are separated by a distance larger than  $R_c$ , the two dressing atoms are not influenced by atom-atom interaction, resulting in an admixed attractive vdW-type interaction  $\nu C_6/|\mathbf{r}-\mathbf{r}'|^6$  between them. When the two atoms are separated at a short distance less than  $R_c$ , the effective potential approaches a constant value because of Rydberg blockade effect.

We choose  $^{87}\text{Rb}$  atoms dressed with the Rydberg levels  $60S_{1/2}$  to realize the soft-core attractive interactions. The dressing of the atoms can be realized by a two-photon transition for the  $5S_{1/2} \rightarrow 6P_{3/2}$  and  $6P_{3/2} \rightarrow 60S_{1/2}$  transitions, respectively. The corresponding Rabi frequencies are given by the overlap with the laser-coupled Rydberg states.

#### APPENDIX B: LEE-HUANG-YANG CORRECTION IN THE BEYOND MEAN-FIELD THEORY

According to the realization of Rydberg dressing, we only need to consider quantum fluctuation induced by the ground-state atoms with contact interaction. We consider ground-state  $^{87}\text{Rb}$  atoms coupled to excited Rydberg  $nS$  state  $^{87}\text{Rb}$  atoms with  $n = 60$  via a Rabi frequency  $\Omega/2\pi = 1$  MHz and a blue laser detuning  $\Delta/2\pi = -100$  MHz. It will then admix a small fraction  $\nu = (\Omega/2\Delta)^2 = 10^{-4}$  of Rydberg character into the ground-state atoms. In this Appendix, we will present in detail the corresponding BdG theory and apply it to homogeneous Rydberg-dressed Bose gases, thereby emphasizing the importance of quantum fluctuations in Rydberg-dressed Bose gases.

To study the Rydberg-dressed system within the BdG theory, we consider the mean-field Hamiltonian  $H_{\text{MF}} = H_{\text{kin}} + H_{\text{int}}$ , which consists of a noninteraction and an interaction contribution. In general, the noninteracting part contains the kinetic energy  $H_{\text{kin}} = \int d^3r \Psi^\dagger(\mathbf{r}) \left[ -\frac{\hbar^2 \nabla^2}{2M} \right] \Psi(\mathbf{r})$ , where  $\Psi^\dagger(\mathbf{r})$  and  $\Psi(\mathbf{r})$  denote the usual bosonic creation and annihilation operators, respectively. Moreover, the interaction is included through  $H_{\text{int}} = \frac{1}{2} \int d^3r d^3r' [\Psi^\dagger(\mathbf{r}) \Psi^\dagger(\mathbf{r}') \Phi(\mathbf{r}-\mathbf{r}') \Psi(\mathbf{r}') \Psi(\mathbf{r})]$ , where  $\Phi(\mathbf{r}-\mathbf{r}') = g\delta(\mathbf{r}-\mathbf{r}')$ .

With Thomas-Fermi approximation, the BdG equation in Fourier space can be written as

$$\begin{aligned} \omega_q u_q(\mathbf{k}) &= \frac{\hbar^2 \mathbf{k}^2}{2M} u_q(\mathbf{k}) + n_0 \Phi(\mathbf{k}) [u_q(\mathbf{k}) + v_q(\mathbf{k})], \\ -\omega_q v_q(\mathbf{k}) &= \frac{\hbar^2 \mathbf{k}^2}{2M} v_q(\mathbf{k}) + n_0 \Phi(\mathbf{k}) [u_q(\mathbf{k}) + v_q(\mathbf{k})], \end{aligned} \quad (\text{B1})$$

where  $n_0$  is the particle density. The Bogoliubov spectrum  $\omega_q = \sqrt{\frac{\hbar^2 \mathbf{k}^2}{2M} + 2n_0 \Phi(\mathbf{k})}$ . The presence of quantum fluctuations also leads to a correction of the ground-state energy of a Rydberg-dressed Bose gas. The total energy can be expressed as

$$E = \frac{1}{2} n_0^2 \Phi(|\mathbf{k}=0|) + \frac{1}{2} V \int \frac{d^3k}{(2\pi)^3} \left[ \omega_q - \frac{\hbar^2 \mathbf{k}^2}{2M} - n_0 \Phi(\mathbf{k}) \right]. \quad (\text{B2})$$

The correction to the ground-state energy  $\Delta E = \frac{2}{5} \gamma_{\text{QF}} n_0^{5/2}$  and the corresponding LHY correction reads  $\gamma_{\text{QF}} = \frac{4M^{3/2} (g - 2\pi^2 |\tilde{C}_6/3R_c^3|)^{5/2}}{3\pi^2 \hbar^3}$  [53].

#### APPENDIX C: DIMENSIONLESS BEYOND GROSS-PITAEVSKII EQUATION AND CALCULATION DETAIL

By introducing the Lee-Huang-Yang correction, one can write a corresponding time-dependent three-dimensional BGPE,

$$i\hbar \frac{\partial \Psi(\mathbf{r}, t)}{\partial t} = \left[ -\frac{\hbar^2}{2M} \nabla^2 + \Phi(\mathbf{r}, t) + \gamma_{\text{QF}} |\Psi(\mathbf{r}, t)|^3 \right] \Psi(\mathbf{r}, t), \quad (\text{C1})$$

where  $\Phi(\mathbf{r}) = g\delta(\mathbf{r}-\mathbf{r}') + \int d^3r' U(\mathbf{r}-\mathbf{r}') |\Psi(\mathbf{r}')|^2$  describes the two-body interactions where the coupling constant  $g$  is related to the  $s$ -wave scattering length  $a_s$  through  $g = \frac{4\pi \hbar^2 a_s}{M}$ ,  $U(\mathbf{r}-\mathbf{r}') = \frac{\tilde{C}_6}{R_c^6+|\mathbf{r}-\mathbf{r}'|^6}$ , with  $\tilde{C}_6 < 0$  and  $R_c$  standing for the effective coupling constant and blockade radius which depends on the details of the Rydberg dressing. The BGPE (C1) can be further transformed into the dimensionless form of Eq. (1) in the main text through  $\Psi(\mathbf{r}, t) = \sqrt{\frac{N}{R_c^3}} \tilde{\Psi}(\tilde{\mathbf{r}}, \tilde{t})$ ,  $t = \frac{MR_c^2}{\hbar} \tilde{t}$  and  $\mathbf{r} = R_c \tilde{\mathbf{r}}$ .

We summarize the numerical method we use in the following three parts:

(a) The nonlocal BGPE of Eq. (1) in the main text is used for the description of the beyond-mean-field ground state of a Rydberg-dressed BEC. The ground state can be described in terms of a single complex order parameter  $\Psi(\mathbf{r}, t)$ , whose squared modulus gives the local density of the system and whose temporal evolution is described by Eq. (1). The ground-state solutions of the system are obtained by using the backward Euler pseudospectral schemes [65] within an imaginary-time propagation approach. For the initial data, we prepare the three-dimensional Gaussian functions as initial wave functions. Fast Fourier transformation (FFT) and inverse fast Fourier transformation (IFFT) are employed to deal with spatial difference and non-local soft-core potential:  $\int \frac{|\Psi(\mathbf{r}')|^2}{1+|\mathbf{r}-\mathbf{r}'|} d\mathbf{r}' = \mathcal{F}^{-1} [\mathcal{F} [\frac{1}{1+r^6}] \mathcal{F} [|\Psi(\mathbf{r})|^2]]$ , where  $\mathcal{F}$  represents FFT and  $\mathcal{F}^{-1}$  represents IFFT [38].

(b) To describe the collective modes of a Rydberg-dressed BEC, we can use a standard Bogoliubov-de Gennes approach and search for a solution of Eq. (1) in the main text of the form  $\Psi(\mathbf{r}, t) = e^{-i\mu t/\hbar} [\Psi_0(\mathbf{r}, t) + \sum_q (u_q(\mathbf{r}) e^{-i\omega_q t/\hbar} - v_q^*(\mathbf{r}) e^{i\omega_q t/\hbar})]$ , with the quasiparticle modes  $u_q, v_q$  and energies  $\omega_q$ . Substituting  $\Psi(\mathbf{r}, t)$  into Eq. (1) and keeping only terms

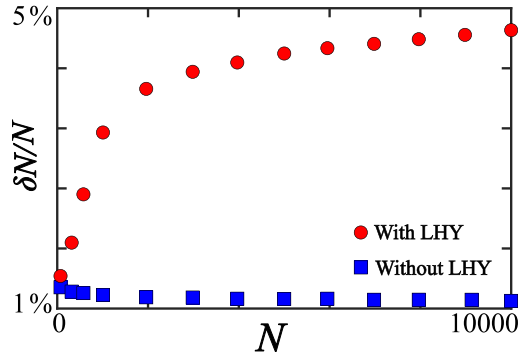


FIG. 5. Quantum depletion  $\delta N/N$  as a function of particle number  $N$  [with (without) LHY correction], where the interaction is fixed as  $\eta = 1/2\pi^2$ .

linear in the quasiparticle amplitudes  $u_q$  and  $v_q$ , we obtain the BdG equations. The ground state  $\Psi_0(\mathbf{r}, t)$  and the chemical potential  $\mu$  are obtained through the imaginary-time evolution. The Bogoliubov excitation energy  $\omega_q$  is numerically obtained by diagonalizing the Bogoliubov Hamiltonian.

(c) To get deeper insight into the physics of the droplet stability, we numerically simulate the dynamics of the collision by means of a real-time evolution of the BGPE Eq. (1). Here we consider the pairwise collision between two droplets moving along the  $x$  direction. The BGPE is usually solved by a

time-splitting method based on the fast Fourier transformation (FFT). We adopt the initial wave function in the superposition state of two droplets propagating in opposite directions and both droplets have the flat-top profile before the collision.

#### APPENDIX D: QUANTUM DEPLETION

The validity of the beyond mean-field approximation can be checked by evaluating the quantum depletion [14]. Based on the Bogoliubov theory, the fluctuation  $\delta\Psi(\mathbf{r}, t)$  around the condensate can be subjected to a canonical transformation leading to the expansion  $\Psi(\mathbf{r}, t) = e^{-i\mu t/\hbar}[\Psi_0(\mathbf{r}, t) + \delta\Psi(\mathbf{r}, t)]$  with  $\delta\Psi(\mathbf{r}, t) = \sum_q [u_q(\mathbf{r})e^{-i\omega_q t/\hbar} - v_q^*(\mathbf{r})e^{i\omega_q t/\hbar}]$ , where  $u_q, v_q$  and energies satisfy the BdG equations [66]

$$\begin{bmatrix} L_{\text{GP}} - \mu + X & -X \\ -X & L_{\text{GP}} - \mu \end{bmatrix} \begin{bmatrix} u_q \\ v_q \end{bmatrix} = \omega_q \begin{bmatrix} u_q \\ v_q \end{bmatrix}, \quad (\text{D1})$$

where the exchange operator  $X$  satisfies  $Xf = \Psi_0(\mathbf{r}) \int d\mathbf{r}' [U(\mathbf{r} - \mathbf{r}')f(\mathbf{r}')\Psi_0^*(\mathbf{r}')] + \frac{3}{2}\gamma_{\text{QF}}|\Psi_0(\mathbf{r})|^3 f$ . The quasiparticles satisfy the normalization relation  $\int d\mathbf{r} [|u_q|^2 - |v_q|^2] = 1$ . At zero temperature, the noncondensate particle number can be calculated by  $\delta N = \int d\mathbf{r} [\sum_q |v_q|^2]$ . Solving the BdG equations in Fourier space, we could present the quantum depletion  $\delta N/N$  as a function of the ground-state particle number  $N$  in Fig. 5. We can see that the quantum depletion is always less than 5%, thereby confirming the validity of the beyond mean-field approximation.

- [1] A. Bulgac, Dilute quantum droplets, *Phys. Rev. Lett.* **89**, 050402 (2002).
- [2] D. S. Petrov, Quantum mechanical stabilization of a collapsing Bose-Bose mixture, *Phys. Rev. Lett.* **115**, 155302 (2015).
- [3] N. B. Jørgensen, G. M. Bruun, and J. J. Arlt, Dilute fluid governed by quantum fluctuations, *Phys. Rev. Lett.* **121**, 173403 (2018).
- [4] T. G. Skov, M. G. Skou, N. B. Jørgensen, and J. J. Arlt, Observation of a Lee-Huang-Yang fluid, *Phys. Rev. Lett.* **126**, 230404 (2021).
- [5] F. Böttcher, J. Schmidt, K. S. H. Ng, S. D. Graham, M. Guo, T. Langen, and T. Pfau, New states of matter with fine-tuned interactions: quantum droplets and dipolar supersolids, *Rep. Prog. Phys.* **84**, 012403 (2021).
- [6] R. Schutzhöhd, M. Uhlmann, Y. Xu, and U. R. Fischer, Mean-field expansion in Bose-Einstein condensates with finite-range interaction, *Int. J. Mod. Phys. B* **20**, 3555 (2006).
- [7] Y. V. Kartashov, B. A. Malomed, and L. Torner, Metastability of quantum droplet clusters, *Phys. Rev. Lett.* **122**, 193902 (2019).
- [8] D. S. Petrov and G. E. Astrakharchik, Ultradilute Low-dimensional liquids, *Phys. Rev. Lett.* **117**, 100401 (2016).
- [9] J. Hertkorn, J.-N. Schmidt, M. Guo, F. Böttcher, K. S. H. Ng, S. D. Graham, P. Uerlings, H. P. Büchler, T. Langen, M. Zwierlein, and T. Pfau, Supersolidity in two-dimensional trapped dipolar droplet arrays, *Phys. Rev. Lett.* **127**, 155301 (2021).
- [10] D. Baillie, R. M. Wilson, and P. B. Blakie, Collective excitations of self-bound droplets of a dipolar quantum fluid, *Phys. Rev. Lett.* **119**, 255302 (2017).
- [11] A. Cidrim, F. E. A. dos Santos, E. A. L. Henn, and T. Macrì, Vortices in self-bound dipolar droplets, *Phys. Rev. A* **98**, 023618 (2018).
- [12] A. Boudjemâa and N. Guebli, Quantum correlations in dipolar droplets: Time-dependent Hartree-Fock-Bogoliubov theory, *Phys. Rev. A* **102**, 023302 (2020).
- [13] A. Boudjemâa, Two-dimensional quantum droplets in dipolar Bose gases, *New J. Phys.* **21**, 093027 (2019).
- [14] A. Boudjemâa, Fluctuations and quantum self-bound droplets in a dipolar Bose-Bose mixture, *Phys. Rev. A* **98**, 033612 (2018).
- [15] G. L. Li, X. D. Jiang, B. Liu, Z. P. Chen, B. A. Malomed, and Y. Y. Li, Two-dimensional anisotropic vortex quantum droplets in dipolar Bose-Einstein condensates, *Front. Phys.* **19**, 22202 (2024).
- [16] M. N. Tengstrand and S. M. Reimann, Droplet-superfluid compounds in binary bosonic mixtures, *Phys. Rev. A* **105**, 033319 (2022).
- [17] L. W. Dong, D. S. Liu, Z. J. Du, K. Shi, and W. Qi, Bistable multiple quantum droplets in binary Bose-Einstein condensates, *Phys. Rev. A* **105**, 033321 (2022).
- [18] M. Caldara and F. Ancilotto, Vortices in quantum droplets of heteronuclear Bose mixtures, *Phys. Rev. A* **105**, 063328 (2022).
- [19] N. Guebli and A. Boudjemâa, Quantum self-bound droplets in Bose-Bose mixtures: Effects of higher-order quantum and thermal fluctuations, *Phys. Rev. A* **104**, 023310 (2021).
- [20] A. Boudjemâa and N. Guebli, Effects of higher-order fluctuations on the bulk and surface properties of quantum droplets in a heteronuclear Bose-Bose mixture, *Phys. Rev. A* **108**, 013305 (2023).

- [21] P. Cheiney, C. R. Cabrera, J. Sanz, B. Naylor, L. Tanzi, M. Inguscio, and L. Tarruell, Bright soliton to quantum droplet transition in a mixture of Bose-Einstein condensates, *Phys. Rev. Lett.* **120**, 135301 (2018).
- [22] G. Semeghini, G. Ferioli, L. Masi, C. Mazzinghi, L. Wolswijk, F. Minardi, M. Modugno, G. Modugno, and M. Fattori, Self-bound quantum droplets of atomic mixtures in free space, *Phys. Rev. Lett.* **120**, 235301 (2018).
- [23] Z. C. Guo, F. Jia, L. T. Li, Y. F. Ma, J. M. Hutson, X. L. Cui, and D. J. Wang, Lee-Huang-Yang effects in the ultracold mixture of  $^{23}\text{Na}$  and  $^{87}\text{Rb}$  with attractive interspecies interactions, *Phys. Rev. Res.* **3**, 033247 (2021).
- [24] I. Ferrier-Barbut, H. Kadau, M. Schmitt, M. Wenzel, and T. Pfau, Observation of quantum droplets in a strongly dipolar Bose gas, *Phys. Rev. Lett.* **116**, 215301 (2016).
- [25] X. L. Cui and Y. F. Ma, Droplet under confinement: Competition and coexistence with a soliton bound state, *Phys. Rev. Res.* **3**, L012027 (2021).
- [26] Y. Li, Z. Luo, Y. Liu, Z. Chen, C. Huang, S. Fu, H. Tan, and B. Malomed, Two-dimensional solitons and quantum droplets supported by competing self- and cross-interactions in spin-orbit-coupled condensates, *New J. Phys.* **19**, 113043 (2017).
- [27] M. N. Tengstrand, P. Stürmer, E. O. Karabulut, and S. M. Reimann, Rotating binary Bose-Einstein condensates and vortex clusters in quantum droplets, *Phys. Rev. Lett.* **123**, 160405 (2019).
- [28] L. W. Dong, B. A. Malomedand, and Y. V. Kartashov, Rotating multidimensional quantum droplets, *Phys. Rev. Lett.* **126**, 244101 (2021).
- [29] M. Tylutki, G. E. Astrakharchik, B. A. Malomed, and D. S. Petrov, Collective excitations of a one-dimensional quantum droplet, *Phys. Rev. A* **101**, 051601(R) (2020).
- [30] H. Hu and X. J. Liu, Collective excitations of a spherical ultradilute quantum droplet, *Phys. Rev. A* **102**, 053303 (2020).
- [31] J. Hertkorn, F. Böttcher, M. Guo, J. N. Schmidt, T. Langen, H. P. Büchler, and T. Pfau, Fate of the amplitude mode in a trapped dipolar supersolid, *Phys. Rev. Lett.* **123**, 193002 (2019).
- [32] G. Natale, R. M. W. van Bijnen, A. Patscheider, D. Petter, M. J. Mark, L. Chomaz, and F. Ferlaino, Excitation spectrum of a trapped dipolar supersolid and its experimental evidence, *Phys. Rev. Lett.* **123**, 050402 (2019).
- [33] S. Sevinçli, N. Henkel, C. Ates, and T. Pohl, Nonlocal nonlinear optics in cold Rydberg gases, *Phys. Rev. Lett.* **107**, 153001 (2011).
- [34] T. Amthor, C. Giese, C. S. Hofmann, and M. Weidemüller, Evidence of antiblockade in an ultracold Rydberg gas, *Phys. Rev. Lett.* **104**, 013001 (2010).
- [35] M. Saffman, T. G. Walker, and K. Mølmer, Quantum information with Rydberg atoms, *Rev. Mod. Phys.* **82**, 2313 (2010).
- [36] F. B. Dunning, T. C. Killian, S. Yoshida, and J. Burgdörfer, Recent advances in Rydberg physics using alkaline-earth atoms, *J. Phys. B: At. Mol. Opt. Phys.* **49**, 112003 (2016).
- [37] N. Henkel, R. Nath, and T. Pohl, Three-dimensional roton excitations and supersolid formation in Rydberg-excited Bose-Einstein condensates, *Phys. Rev. Lett.* **104**, 195302 (2010).
- [38] W. Han, X. F. Zhang, D. S. Wang, H. F. Jiang, W. Zhang, and S. G. Zhang, Chiral supersolid in spin-orbit-coupled Bose gases with soft-core long-range interactions, *Phys. Rev. Lett.* **121**, 030404 (2018).
- [39] M. Burrello, I. Lesanovsky, and A. Trombettoni, Reaching the quantum Hall regime with rotating Rydberg-dressed atoms, *Phys. Rev. Res.* **2**, 023290 (2020).
- [40] I. Seydi, S. H. Abedinpour, R. E. Zillich, R. Asgari, and B. Tanatar, Rotons and Bose condensation in Rydberg-dressed Bose gas, *Phys. Rev. A* **101**, 013628 (2020).
- [41] J. B. Balewski, A. T. Krupp, A. Gaj, S. Hofferberth, R. Løw, and T. Pfau, Rydberg dressing: understanding of collective many-body effects and implications for experiments, *New J. Phys.* **16**, 063012 (2014).
- [42] S. Weber, C. Tresp, H. Menke, A. Urvoy, O. Firstenberg, H. P. Büchler, and S. Hofferberth, Calculation of Rydberg interaction potentials, *J. Phys. B: At. Mol. Opt. Phys.* **50**, 133001 (2017).
- [43] X. Wu, X. Liang, Y. Tian, F. Yang, C. Chen, Y. Liu, M. Tey, and L. You, A concise review of Rydberg atom based quantum computation and quantum simulation, *Chin. Phys. B* **30**, 020305 (2021).
- [44] J. Honer, H. Weimer, T. Pfau, and H. P. Büchler, Collective many-body interaction in Rydberg dressed atoms, *Phys. Rev. Lett.* **105**, 160404 (2010).
- [45] F. Maucher, N. Henkel, M. Saffman, W. Królikowski, S. Skupin, and T. Pohl, Rydberg-induced solitons: Three-dimensional self-trapping of matter waves, *Phys. Rev. Lett.* **106**, 170401 (2011).
- [46] C.-H. Hsueh, Y.-C. Tsai, K.-S. Wu, M.-S. Chang, and W. C. Wu, Pseudospin orders in the supersolid phases in binary Rydberg-dressed Bose-Einstein condensates, *Phys. Rev. A* **88**, 043646 (2013).
- [47] C.-H. Hsueh, T.-C. Lin, T.-L. Horng, and W. C. Wu, Pseudospin orders in the supersolid phases in binary Rydberg-dressed Bose-Einstein condensates, *Phys. Rev. A* **86**, 013619 (2012).
- [48] L. Lavoine, A. Hammond, A. Recati, D. S. Petrov, and T. Bourdel, Pseudospin orders in the supersolid phases in binary Rydberg-dressed Bose-Einstein condensates, *Phys. Rev. Lett.* **127**, 203402 (2021).
- [49] T. D. Lee, K. Huang, and C. N. Yang, Eigenvalues and eigenfunctions of a Bose system of hard spheres and its low-temperature properties, *Phys. Rev.* **106**, 1135 (1957).
- [50] S. Pal, D. Baillie, and P. B. Blakie, Infinite dipolar droplet: A simple theory for the macrodroplet regime, *Phys. Rev. A* **105**, 023308 (2022).
- [51] F. Wächtler and L. Santos, Quantum filaments in dipolar Bose-Einstein condensates, *Phys. Rev. A* **93**, 061603 (2016).
- [52] F. Ancilotto, M. Rossi, and F. Toigo, Supersolid structure and excitation spectrum of soft-core bosons in three dimensions, *Phys. Rev. A* **88**, 033618 (2013).
- [53] C.-H. Hsueh, C.-W. Wang, and W.-C. Wu, Vortex structures in a rotating Rydberg-dressed Bose-Einstein condensate with the Lee-Huang-Yang correction, *Phys. Rev. A* **102**, 063307 (2020).
- [54] Y. Y. Li, Z. P. Chen, Z. H. Luo, C. Q. Huang, H. S. Tan, W. Pang, and B. A. Malomed, Vortex structures in a rotating Rydberg-dressed Bose-Einstein condensate with the Lee-Huang-Yang correction, *Phys. Rev. A* **98**, 063602 (2018).
- [55] L. Bergé, Wave collapse in physics: principles and applications to light and plasma waves, *Phys. Rep.* **303**, 259 (1998).
- [56] G. Ferioli, G. Semeghini, L. Masi, G. Giusti, G. Modugno, M. Inguscio, A. Gallemlí, A. Recati, and M. Fattori, Collisions of self-bound quantum droplets, *Phys. Rev. Lett.* **122**, 090401 (2019).



- [57] M. Barbier, H. Lütjeharms, and W. Hofstetter, Supersolid phases of ultracold bosons trapped in optical lattices dressed with Rydberg  $p$  states, *Phys. Rev. A* **105**, 013326 (2022).
- [58] C.-Y. Huang, J. P. Zhuang, P.-Y. Chang, and D.-W. Wang, Two-dimensional paired topological superfluids of Rydberg Fermi gases, *Phys. Rev. B* **106**, 024506 (2022).
- [59] Y. J. Zhou, R. Nath, H. B. Wu, I. Lesanovsky, and W. B. Li, Multipolar Fermi-surface deformation in a Rydberg-dressed Fermi gas with long-range anisotropic interactions, *Phys. Rev. A* **104**, L061302 (2021).
- [60] M. Pi, F. Ancilotto, J. M. Escartín, R. Mayol, and M. Barranco, Rotating mixed  $^3\text{He}$ - $^4\text{He}$  nanodroplets, *Phys. Rev. B* **102**, 060502(R) (2020).
- [61] L. A. Peña Ardila and T. Pohl, Ground-state properties of dipolar Bose polarons, *J. Phys. B: At. Mol. Opt. Phys.* **52**, 015004 (2019).
- [62] J. R. Li, W. J. Huang, B. Shteynas, S. Burchesky, F. C. Top, E. Su, J. Lee, A. O. Jamison, and W. Ketterle, Spin-orbit coupling and spin textures in optical superlattices, *Phys. Rev. Lett.* **117**, 185301 (2016).
- [63] H. Zhu, C. F. Liu, D. S. Wang, S. G. Yin, L. Zhuang, and W. M. Liu, Spin-orbit coupling controlling the topological vortical phase transition in spin-2 rotating Bose-Einstein condensates, *Phys. Rev. A* **104**, 053325 (2021).
- [64] D. F. Zhang, T. Y. Gao, P. Zou, L. R. Kong, R. Z. Li, X. Shen, X. L. Chen, S. G. Peng, M. S. Zhang, H. Pu, and K. J. Jiang, Ground-state phase diagram of a spin-orbital-angular-momentum coupled Bose-Einstein condensate, *Phys. Rev. Lett.* **122**, 110402 (2019).
- [65] W. Han, G. Juzeliūnas, W. Zhang, and W. M. Liu, Supersolid with nontrivial topological spin textures in spin-orbit-coupled Bose gases, *Phys. Rev. A* **91**, 013607 (2015).
- [66] T. Macrì, F. Maucher, F. Cinti, and T. Pohl, Elementary excitations of ultracold soft-core bosons across the superfluid-supersolid phase transition, *Phys. Rev. A* **87**, 061602(R) (2013).